CMS Physics Analysis Summary

Contact: cms-pag-conveners-exotica@cern.ch

2015/12/15

Searches for Long-lived Charged Particles in Proton-Proton Collisions at $\sqrt{s} = 13$ TeV

The CMS Collaboration

Abstract

The results of searches for heavy stable charged particles produced in pp collisions at $\sqrt{s} = 13$ TeV corresponding to an integrated luminosity of 2.4 fb^{-1} are presented. Candidates are searched for in data collected with the CMS detector at the CERN LHC by using signatures of anomalously high energy deposition in the silicon tracker and long time-of-flight to the muon detectors. The data are consistent with the expected background and limits on the cross section for production of long-lived gluinos, scalar tops and taus are set. Corresponding lower mass limits, ranging up to 1590 GeV for gluinos, are the most stringent to date. Limits on the cross section for direct pair production of scalar taus and lepton-like long-lived fermions are also set.

1 Introduction

Many extensions of the standard model (SM) include heavy, long-lived, charged particles that have speed, v, significantly less than the speed of light, c, [1–3] and/or charge, Q, not equal to $\pm 1e$ [4–7]. With lifetimes greater than a few nanoseconds, these particles can travel distances larger than the typical collider detector and appear stable like the pion or kaon. These particles can be generically referred to as heavy stable charged particles (HSCPs) and can be singly charged ($|Q| = 1e$), fractionally charged ($|Q| < 1e$), or multiply charged ($|Q| > 1e$). Without dedicated searches, HSCPs may be mis-identified or unobserved as particle identification algorithms at hadron collider experiments generally assume signatures characteristic of SM particles, e.g., speed close to the speed of light and a charge of 0 or $\pm 1e$. Additionally, HSCPs may be charged during only part of their passage through detectors, further limiting the ability of standard algorithms to identify them.

For HSCP masses greater than $\gtrsim 100$ GeV, a significant fraction of particles produced at the CERN LHC will have velocity, $\beta \equiv v/c$, less than 0.9. It is possible to distinguish $|Q| \geq 1e$ particles with $\beta < 0.9$ from speed-of-light SM particles through their higher rate of energy loss via ionization (dE/dx) and/or through their longer time-of-flight (TOF) to the outer detectors.

The dependence of dE/dx on particle momentum is described by the Bethe-Bloch formula [8]. This dependence can be seen in Fig. 1, which shows dE/dx versus momentum for tracks from data and simulated HSCP signals with various charges. In the momentum range of interest at the LHC (10–1000 GeV), SM particles interact with nearly flat ionization energy loss (≈ 3 MeV/cm). Searching for candidates with larger dE/dx gives sensitivity to massive particles with $|Q| = 1e$ and particles with $|Q| > 1e$.

Previous collider searches for HSCPs have been performed at LEP [9–12], HERA [13], the Tevatron [14–17], and the LHC [18–25]. The results from these searches have placed significant bounds on beyond the standard model theories [26, 27], such as lower limits at 95% confidence level on the mass of gluinos, scalar top quarks, and pair produced scalar tau at 1098, 737, and 223 GeV, respectively. Presented here are several searches for singly and multiply charged HSCPs in data collected with the CMS detector at $\sqrt{s} = 13$ TeV in 2015.

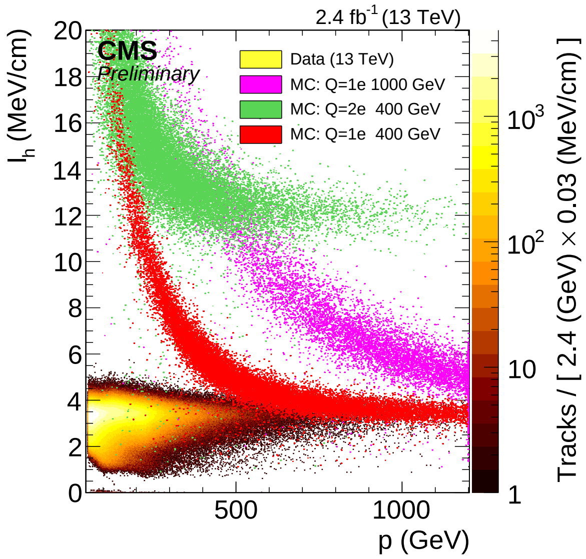

Figure 1: Distribution of the dE/dx estimator, I_h (see Section 3.1), versus particle momentum for 13 TeV data, and for singly or multiply charged HSCP simulation.

2 Signal Benchmarks

This search employs several types of signal model to account for the numerous different types of HSCP that are theoretically allowed.

The first type of signal consists of HSCPs that interact via the strong force and hadronize with SM quarks to form *R*-hadrons. As in Ref. [28], events involving pair production of $\widetilde{g}$ and $\widetilde{t}_1$, with mass values in the range 300-2600 GeV, are generated under the Split SUSY scenarios. Gluinos are generated under the high squark mass (10 TeV) assumption. PYTHIA v8.153 [29] with the default tune CUETP8M1 is used to generate the 13 TeV Monte Carlo (MC) samples. The fraction, f, of produced $\widetilde{g}$ hadronizing into a $\widetilde{g}$-gluon state (*R*-gluonball) is an unknown parameter of the hadronization model and affects the fraction of *R*-hadrons that are neutral at production. For this search, results are obtained for two different values of f, 0.1 and 0.5. Unless otherwise specified, the value $f = 0.1$ should be assumed. As in Ref. [28], two scenarios of *R*-hadron strong interactions with matter are considered: the first follows the model in Refs. [30, 31] while the second is one of complete charge suppression, where each nuclear interaction experienced by the *R*-hadron causes it to become neutral. Both the tracker-only and tracker+TOF analyses are used to search for these signals, but the tracker-only analysis is expected to have sensitivity even in the charge suppression scenario.

The second type of signal consists of HSCPs that behave like leptons. The minimal gauge mediated supersymmetry breaking (mGMSB) model [32] is selected as a benchmark for lepton-like HSCPs. Production of supersymmetric quasi-stable leptons ($\tilde{\tau}_1$) at the LHC can proceed either directly or via production of heavier supersymmetric particles (mainly squarks and gluino pairs) that decay, leading to one or more $\tilde{\tau}_1$ particles at the end of the decay chain. The latter process is generally dominant because of the electroweak nature of the direct production process. The mGMSB model is explored using the SPS7 slope [33], which has the stau ($\tilde{\tau}$) as the next-to-lightest supersymmetric particle (NLSP). The particle mass spectrum and the decay table are produced with the program ISASUGRA [34] version 7.69. The mGMSB parameter Λ is varied from 31 to 160 TeV, with fixed parameters $N_{\text{mes}} = 3$, $\tan\beta = 10$, $\mu > 0$, $C_{\text{grav}} = 10000$, and $M_{\text{mes}}/\Lambda = 2$. The large value of C_{grav} results in a long-lived stau, while Λ = 31–510 TeV gives a stau mass of 100 to 1600 GeV. The produced SUSY mass spectrum is input to PYTHIA v6.4 [29] with Z2star tune as the generator for a MC simulation at 13 TeV. Two $\widetilde{\tau}$ samples are generated for each SUSY point: one with all processes (labeled "GMSB stau") and one with only direct pair production (labeled "Pair Prod. stau"). The pair-produced stau includes only $\tilde{\tau}_1$, which is predominantly $\tilde{\tau}_R$ for these model parameters. The tracker-only and tracker+TOF analyses are both used to search for these signals.

The last type of signal are based on modified Drell–Yan production of long-lived lepton-like fermions. In this scenario, new massive spin-1/2 particles have arbitrary electric charge but are neutral under SU(3)C and SU(2)L, and therefore couple only to the photon and the Z boson. PYTHIA v6.4 [29] with Z2star tune is used to generate the 13 TeV Monte Carlo (MC) signal samples. Simulations are generated for lepton-like fermions with masses ranging from 100 to 2600 GeV and for electric charges $|Q|$ = e and 2e.

Different PYTHIA tunes used in generating the samples above were studied and the effects on kinematic distributions for the HSCPs considered were negligible. The tracker-only and tracker+TOF analyses are both expected to have sensitivity to $|Q| = 2e$ HSCPs.

In all signal samples, simulated minimum bias events are overlaid with the primary collision to produce the effect of multiple interactions per bunch crossing (pileup).

3 CMS Detector

The central feature of the CMS apparatus is a superconducting solenoid of 6 m internal diameter. Within the superconducting solenoid volume are a silicon pixel and strip tracker, a lead tungstate crystal electromagnetic calorimeter (ECAL), and a brass and scintillator hadron calorimeter (HCAL), each composed of a barrel and two endcap sections. Forward calorimeters extend the pseudorapidity [35] coverage provided by the barrel and endcap detectors. Muons are measured in gas-ionization detectors embedded in the steel flux-return yoke outside the solenoid. The missing transverse momentum vector $\vec{p}_{\mathrm{T}}^{\mathrm{miss}}$ is defined as the projection on the plane perpendicular to the beams of the negative vector sum of the momenta of all reconstructed particles in an event. Its magnitude is referred to as $E_{\mathrm{T}}^{\mathrm{miss}}$.

The silicon tracker measures charged particles within the pseudorapidity range $|\eta| < 2.5$. It consists of 1440 silicon pixel and 15 148 silicon strip detector modules and is located in the 3.8 T field of the superconducting solenoid. Isolated particles of $p_{\mathrm{T}} = 100\,\mathrm{GeV}$ emitted at $|\eta| < 1.4$ have track resolutions of 2.8% in p_{T} and 10 (30) μm in the transverse (longitudinal) impact parameter [36]. Muons are measured in the pseudorapidity range $|\eta| < 2.4$, with detection planes made using three technologies: drift tubes (DTs), cathode strip chambers (CSCs), and resistive plate chambers (RPCs). Matching muons to tracks measured in the silicon tracker results in a relative transverse momentum resolution for muons with $20 < p_{\mathrm{T}} < 100\,\mathrm{GeV}$ of 1.3–2.0% in the barrel and better than 6% in the endcaps, The p_{T} resolution in the barrel is better than 10% for muons with p_{T} up to 1 TeV [37]. The first level (L1) of the CMS trigger system, composed of custom hardware processors, uses information from the calorimeters and muon detectors to select the most interesting events in a fixed time interval of less than 4 μs. The high-level trigger (HLT) processor farm further decreases the event rate from around 100 kHz to less than 1 kHz, before data storage. A more detailed description of the CMS detector, together with a definition of the coordinate system used and the relevant kinematic variables, can be found in Ref. [35].

3.1 dE/dx Measurements

As in Ref. [23], a dE/dx discriminator, I_{as} is used to distinguish SM particles from HSCP candidates. The discriminator is a probability and is given by:

$$I_{as} = \frac{3}{N} \times \left(\frac{1}{12N} + \sum_{i=1}^{N} \left[P_i \times \left(P_i - \frac{2i-1}{2N} \right)^2 \right] \right), \tag{1}$$

where N is the number of measurements in the silicon-tracker detectors, P_i is the probability for a minimum–ionizing particle to produce a charge smaller or equal to that of the i–th measurement for the observed path length in the detector, and the sum is over the track measurements ordered in terms of increasing P_i.

In addition, the dE/dx of a track is estimated using a harmonic-2 estimator:

$$I_h = \left(\frac{1}{N} \sum_{i}^{N} c_i^{-2} \right)^{-1/2}, \tag{2}$$

where c_i is the charge per unit path length in the sensitive part of the silicon detector of the i-th track measurement. The harmonic-2 estimator has units MeV/cm and, as for I_{as} the sum includes both pixel and strip silicon detectors.

The mass of a candidate particle can be calculated [28], from its momentum and I_h dE/dx estimate, based on the relationship :

$$I_h = K\frac{m^2}{p^2} + C. \quad (3)$$

where the empirical parameters $K = 2.535 \pm 0.001\,\mathrm{MeV\ cm^{-1}}$ and $C = 3.339 \pm 0.001\,\mathrm{MeV\ cm^{-1}}$ are determined from data using a sample of low-momentum protons. As the momentum reconstruction is done assuming $|Q| = 1e$ particles, the relation above would lead to a proper mass reconstruction only for singly charged particles.

The HSCP candidates are primarily selected using the I_{as} discriminator (see Sec. 5) because it has a higher signal-to-background discriminating power in comparison to the I_h estimator or the mass. Nonetheless, the mass is used at the last stage of the analysis, after the I_{as} selection, to further discriminate between signal and backgrounds since the latter tend to have a low reconstructed mass.

3.2 Time-of-flight Measurements

The time-of-flight to the muon system can be used to discriminate between near speed-of-light particles and slower candidates. A single δ_t measurement can be used to determine the track β^{-1} via the equation:

$$\beta^{-1} = 1 + \frac{c\delta_t}{L} \quad (4)$$

where L is the flight distance. The track β^{-1} value is calculated as the weighted average of the β^{-1} measurements from the DT and CSC systems associated with the track. The weight for the i^{th} DT measurement is given by:

$$w_i = \frac{(n-2)}{n}\frac{L_i^2}{\sigma_{DT}^2} \quad (5)$$

where n is the number of ϕ projection measurements found in the muon chamber from which the measurement comes and σ_{DT} is the time resolution of the DT measurements, for which the measured value of 3 ns is used. The factor $(n-2)/n$ accounts for the fact that residuals are computed using two parameters of a straight line determined from the same n measurements (minimal number of hits in a given DT chamber that allows for at least one residual calculation is $n = 3$). The weight for the i^{th} CSC measurement is given by:

$$w_i = \frac{L_i^2}{\sigma_i^2} \quad (6)$$

where σ_i, the measured time resolution, is 7.0 ns for cathode strip measurements and 8.6 ns for anode wire measurements.

The resolution on the weighted average β^{-1} measurement is approximately 0.065 in both the DT and CSC subsystems.

4 Data Selection

HSCPs are searched for in two ways: (1) requiring tracks to be reconstructed in both the silicon detectors and the muon system, referred to as the “tracker+TOF” analysis; (2) only requiring tracks be reconstructed in the silicon detectors, the “tracker-only” analysis.

All events are required to pass a trigger requiring either the reconstruction of a muon with high transverse momentum or the calculation of large $E_{\mathrm{T}}^{\mathrm{miss}}$ using an online particle-flow algorithm [38].

The muon trigger is more efficient than the $E_{\mathrm{T}}^{\mathrm{miss}}$ trigger for all HSCP models with the exception of the charged suppressed R-hadron model, but it is not efficient for particles that are too slow ($\beta < 0.6$).

The $E_{\mathrm{T}}^{\mathrm{miss}}$ trigger can recover some events in which the HSCP is charged in the tracker and neutral in the muon subsystem. The particle-flow algorithm rejects tracks reconstructed only in the tracker with a track p_T much greater than the matched energy deposited in the calorimeter [39], as would be the case for HSCPs that become neutral in the calorimeter. Thus only the energy these HSCPs deposit in the calorimeter, roughly 10–20 GeV, will be included in the $E_{\mathrm{T}}^{\mathrm{miss}}$ calculation. Significant $E_{\mathrm{T}}^{\mathrm{miss}}$ can results in events where one or more HSCPs fail to be reconstructed as muon candidates.

For both analyses, the muon trigger requires $p_{\mathrm{T}} > 50\,\mathrm{GeV}$ and the $E_{\mathrm{T}}^{\mathrm{miss}}$ trigger requires $E_{\mathrm{T}}^{\mathrm{miss}}$ $> 170\,\mathrm{GeV}$. Using multiple triggers for both analyses allows for increased sensitivity to HSCP candidates that arrive in the muon system very late as well as for hadron-like HSCPs, which are sometimes charged only in the tracker.

For the tracker-only analysis, all events are required to have a candidate track with $p_{\mathrm{T}} > 55$ GeV (as measured in the tracker), relative uncertainty on p_{T} ($\sigma_{p_{\mathrm{T}}}/p_{\mathrm{T}}$) less than 0.25, $|\eta| < 2.1$, track fit $\chi^2/\mathrm{dof} < 5$, and magnitudes of the impact parameters d_z and d_{xy} both less than 0.5 cm (d_z and d_{xy} are the longitudinal and transverse impact parameters with respect to the vertex with the minimal d_z). The cuts on the impact parameters are very loose compared to the resolutions for tracks in the tracker. Candidates must pass isolation requirements in the tracker and calorimeter. The tracker isolation criteria is $\Sigma p_T < 50\,\mathrm{GeV}$, where the sum is over all tracks (except the candidate) within $\Delta R = \sqrt{(\Delta\eta)^2 + (\Delta\phi)^2} < 0.3$. The calorimeter isolation criteria is $E/p < 0.3$, where E is the sum of energy deposited in the calorimeter towers within $\Delta R < 0.3$ and p is the track momentum reconstructed from the tracker. Candidates must have at least two measurements in the silicon pixel detector and at least six measurements in the strip detectors. In addition, there must be measurements in at least 80% of the silicon layers between the first and last measurements of the track. To reduce the rate of contamination from clusters with large energy deposition due to overlapping tracks, a cleaning procedure is applied to remove clusters in the silicon strip tracker that are not consistent with the passage of a single charged particle (e.g., a narrow cluster with most of the energy deposited in one or two strips). After cluster cleaning, there must be at least six measurements in the silicon tracker that are used for the dE/dx calculation.

The tracker+TOF analysis applies the same criteria, but additionally requires a reconstructed muon matched to the track in the inner detectors. At least eight independent time measurements are needed for the TOF computation. Finally, $1/\beta > 1$ and $\sigma_{1/\beta} < 0.15$ are required.

5 Background Prediction

For both analyses, results are based upon a comparison of the number of candidates passing the selection criteria defining the signal region (see Section 7) with the number of predicted background events in that region. Candidates passing the preselection criteria (Section 4) are subject to two (or three) additional criteria to improve the signal-to-background discrimination. By choosing criteria that are uncorrelated, it is possible to use the candidates that fail one (or more) of these criteria to predict the background with the $ABCD$ method where D, the background expectation in the signal region, is estimated by $D = BC/A$, where B and C are, respectively, the number of candidates that fail the first and second criteria, respectively, but pass the other one, while A is the number of candidates that fail both criteria.

For the tracker-only analysis, the two chosen criteria are $p_{\mathrm{T}} > 65\,\mathrm{GeV}$ and $I_{as} > 0.3$. The candidates passing only the I_{as} requirement fall into the B region and those passing only the p_{T} requirement fall into the C region. The B and C candidates are then used to form a binned probability density function in I_h and p, respectively, such that, using the mass determination (Eq. (3)), the full mass spectrum of the background in the signal region D can be predicted. However, the η distribution of candidates at low dE/dx differs from the distribution of the candidates at high dE/dx. To correct for this, events in the C region are weighted such that the η distribution matches that in the B region.

For the tracker+TOF analysis, three criteria are used, $p_{\mathrm{T}} > 65\,\mathrm{GeV}$, $I_{as} > 0.175$, and $1/\beta > 1.250$, creating eight regions labeled $A - H$. Region D represents the signal region, with events passing all three criteria. The candidates in the A, F, and G regions pass only the $1/\beta$, I_{as}, and p_{T} criteria, respectively, while the candidates in the B, C, and H regions fail only the p_{T}, I_{as}, and $1/\beta$ criteria, respectively. The E region contains events that fail all three criteria. Background estimates can be made from several different combinations of these regions. The combination $D = AGF/E^2$ is used because it yields the smallest statistical uncertainty. As in the tracker-only analysis, events in the G region are reweighted to match the η distribution in the B region. The spread in background estimates from the other combinations is less than 20%, which is taken as the systematic uncertainty in the background estimate. The same 20% systematic uncertainty is used for the tracker-only analysis.

In order to check the background prediction, samples with a loose selection, which would be dominated by background tracks, are used for the tracker-only and tracker+TOF analyses. The loose selection sample for the tracker-only analysis is defined as $p_T > 60\,\mathrm{GeV}$ and $I_{as} > 0.10$. The loose selection sample for the tracker+TOF analysis is defined as $p_T > 60\,\mathrm{GeV}$, $I_{as} > 0.05$, and $1/\beta > 1.05$. Figure 2 shows the observed and predicted mass spectra for these samples.

For each analysis, fixed selections on the appropriate set of I_{as}, p_{T}, and $1/\beta$ are used to define the final signal region (and the regions for the background prediction). These values are chosen to give the best discovery potential over the signal mass regions of interest. For both analyses, an additional requirement on the reconstructed mass is applied. The specific requirement is adapted to each HSCP model. For a given mass and model, the mass requirement is $M \geq M_{reco} - 2\sigma$ where M_{reco} is the average reconstructed mass for the given mass M_{HSCP} and σ is the expected resolution. Simulation is used to determine M_{reco} and σ.

Table 1 lists the final selection criteria, the predicted number of background events, and the number of events observed in the signal region. Agreement between prediction and observation is seen for both tracker-only and tracker+TOF analyses. Figure 3 shows the observed and predicted mass distribution for the tracker-only and tracker+TOF analyses with the final selection.

6 Systematic Uncertainties

The considered sources of systematic uncertainty are those related to the integrated luminosity, the background prediction, and the signal efficiency. The uncertainty on the integrated luminosity is 4.6% at $\sqrt{s} = 13$ TeV. The uncertainties on the background predictions are described

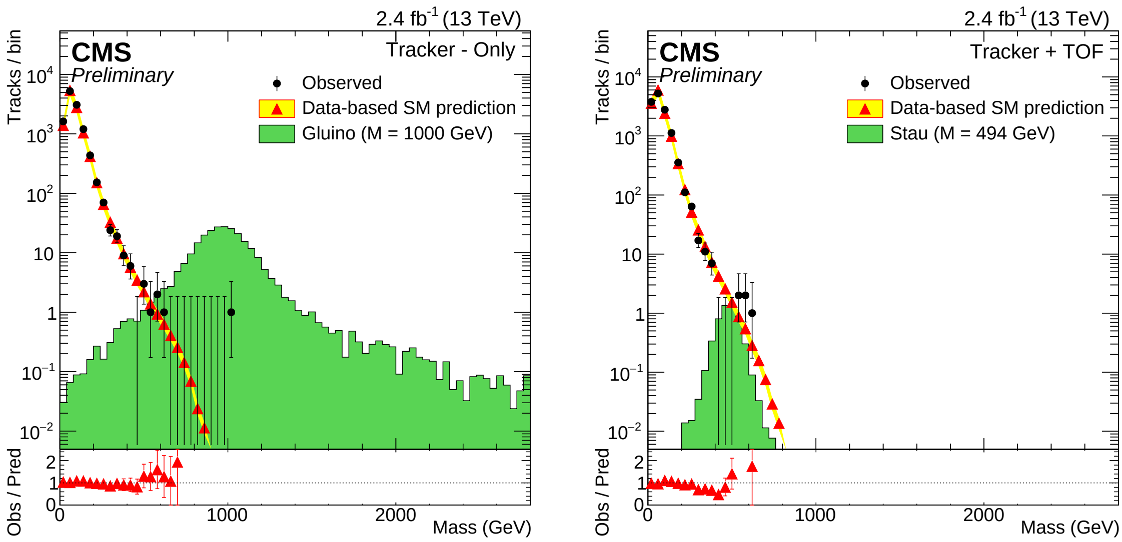

Figure 2: Observed and predicted mass spectra for candidates entering the tracker-only (left) and tracker+TOF (right) signal region for the loose selection for $\sqrt{s} = 13$ TeV. The expected distribution for a representative signal is shown in green.

Table 1: Selection criteria for the various subanalyses with number of predicted and observed events at 13 TeV.

	Selection cuts				Number of events $\sqrt{s} = 13$ TeV	
	p_T (GeV)	I_{as}	$1/\beta$	Mass (GeV)	Pred.	Obs.
Trk-only	> 65	> 0.3	-	> 0	28.8 ± 6.1	24
				> 100	17.8 ± 3.8	13
				> 200	2.6 ± 0.6	2
				> 300	0.53 ± 0.12	0
				> 400	0.16 ± 0.035	0
Trk+TOF	> 65	> 0.175	> 1.250	> 0	17.9 ± 3.6	13
				> 100	4.1 ± 0.8	3
				> 200	0.60 ± 0.12	0
				> 300	0.12 ± 0.024	0

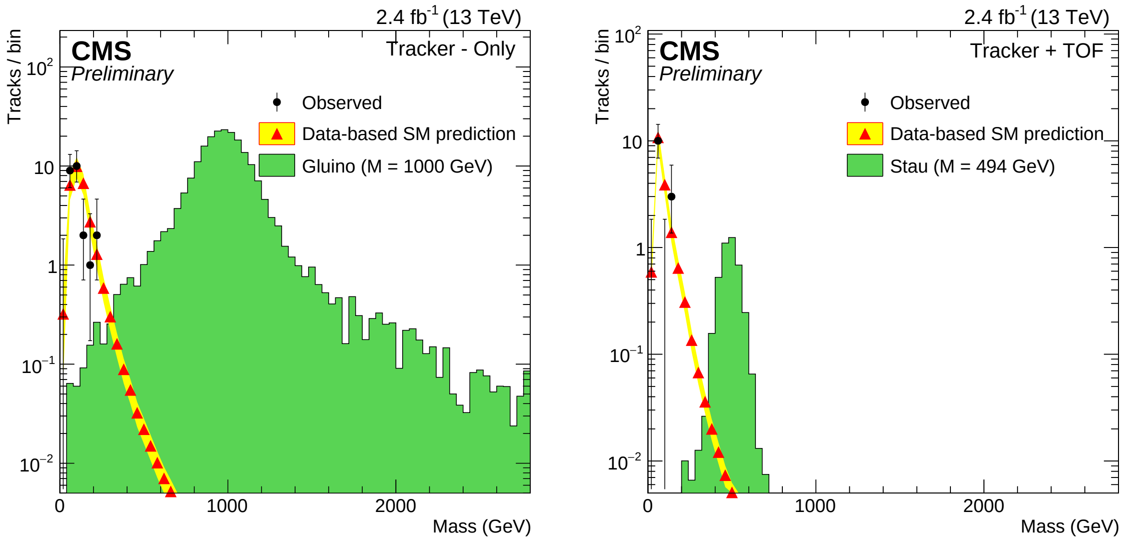

Figure 3: Observed and predicted mass spectra for candidates entering the tracker-only (left) or tracker+TOF (right) signal region for the final selection. The expected distribution for a representative signal is shown in green.

in Section 5.

The signal efficiency is obtained from Monte Carlo simulations of the various signals processed through the full detector simulation (Section 2). Systematic uncertainties on the final results are driven by uncertainties on the differences between the simulation and data. The relevant differences are discussed below.

The signal trigger efficiency is dominated by the muon triggers for all the models except the charge-suppressed ones. The uncertainty on the muon trigger efficiency has many contributions. The trigger efficiency in MC and data varies by up to 3%. For slow moving particles, the effect of timing synchronization of the muon system is tested by shifting the arrival times in MC by the synchronization accuracy observed in data, resulting in an efficiency change of less than 4% for most samples and up to 8% for the 2.4 TeV gluino. The uncertainty in the $E_{\mathrm{T}}^{\mathrm{miss}}$ trigger efficiency is found by varying the jet energy scale in the simulation of the HLT by its uncertainty in data. The $E_{\mathrm{T}}^{\mathrm{miss}}$ uncertainty is found to be less than 12% for all samples. The total trigger uncertainty is found to be less than 13% for all the samples since the muon trigger inefficiencies are often compensated by the $E_{\mathrm{T}}^{\mathrm{miss}}$ trigger and vice versa.

Low momentum protons are used to quantify the agreement between the observed and simulated distributions, I_h and I_{as}, resulting from energy loss in the silicon tracker. The dE/dx distributions of signal samples are varied by the observed differences in order to estimate the systematic uncertainty. The uncertainty in the signal acceptance is usually less than 10%, and is at most 15%.

Bias in the energy loss measurement caused by highly ionizing particles (HIP) such as low momentum protons produced in pp collisions earlier than the triggering collision was also considered as a source of uncertainty in the I_h estimate. The HIP background was added in the MC with a rate corresponding to the level observed during the 2015 data taking. This leads to a change in signal efficiency of up to 25% and 30% for the tracker-only and tracker+TOF analyses, respectively.

Table 2: Systematic uncertainties for the various HSCP searches. All values are relative uncertainties.

Source of Systematic Uncertainties	Relative Uncertainty (%)	
Signal acceptance	Trk-only	Trk+TOF
- Trigger efficiency	13	13
- Track momentum scale	< 20	< 20
- Track reconstruction	< 2	< 2
- Ionization energy loss	< 15	< 15
- HIP background	< 25	< 30
- Time-of-flight	-	< 5
- Muon reconstruction	-	2
- Pileup	< 1	< 1
Total uncertainty on signal acceptance	< 35	< 50
Background uncertainty	20	20
Luminosity uncertainty	4.6	

Dimuon events are used to test the MC simulation of $1/\beta$ by comparing to data. An offset of at most 1.5% is found for the muon system. The resulting uncertainty in the signal acceptance is found to be less than 5% by shifting $1/\beta$ by this amount.

As in Ref. [25], the uncertainties on the efficiencies for muon reconstruction [37] and track reconstruction [40] are less than 2% each. The track momentum uncertainty is estimated by shifting the momentum from the inner track as in Ref. [25]. This uncertainty is found to be less than 5% for most of the samples, increasing to 20% for masses above 2 TeV.

The uncertainty in the number of pileup events is evaluated using a 5% variation in the minimum bias cross section used to calculate the weights applied to signal events in order to reproduce the pileup observed in data. This results in uncertainties due to pileup of less than 1%.

The total systematic uncertainty in the signal efficiency is the sum in quadrature of the uncertainties due to the sources discussed above. For all the samples, it is less than 35% for the tracker-only analysis and less than 50% for the tracker+TOF analysis.

Table 2 summarizes the systematic uncertainties for the two analyses. As the uncertainty often depends on the model and HSCP mass, the largest systematic uncertainty is reported for each source.

7 Results

No significant excess of events is observed above the predicted background. Cross section limits are placed at 95% confidence level (CL) using a CLs approach [41, 42] where p-values are computed with a profile likelihood technique [43] that uses a lognormal model [44, 45] for the nuisance parameters. The latter are the integrated luminosity, the signal acceptance, and the expected background in the signal region. The observed limits are shown in Fig. 4 for both tracker-only and tracker+TOF analyses along with the theoretical predictions. For the gluino and stop pair production, the theoretical cross sections are computed at NLO+NLL [46–49] using PROSPINO [50] with CTEQ6.6M PDFs [51]. The uncertainty bands on the theoretical cross sections include the PDF uncertainty as well as the μ and α_s scale uncertainties. Mass limits are

Table 3: Summary of the p_T, I_{as}, $1/\beta$, and mass thresholds, the observed and predicted yields passing these criteria, and the resulting expected (Exp.) and observed (Obs.) cross section limits for gluino signals. The signal efficiency and theoretical (Th.) cross section are also listed.

Mass	Requirements				Yields		Signal	σ (pb)		
	p_T (GeV)	I_{as}	$1/\beta$	M (GeV)	Predicted	Data	Eff.	Th.	Exp.	Obs.
Gluino ($f = 0.1$) particles with the tracker-only analysis										
400	65	0.300	/	40	28.400 $\pm$ 6.070	24	0.166	9.5E+01	3.8E-02	3.0E-02
800	65	0.300	/	330	0.359 $\pm$ 0.079	0	0.221	1.5E+00	5.8E-03	5.8E-03
1200	65	0.300	/	580	0.030 $\pm$ 0.007	0	0.217	8.4E-02	6.0E-03	6.0E-03
1600	65	0.300	/	710	0.010 $\pm$ 0.002	0	0.156	8.0E-03	8.4E-03	8.4E-03
2000	65	0.300	/	750	0.007 $\pm$ 0.002	0	0.079	9.7E-04	1.6E-02	1.6E-02
2400	65	0.300	/	730	0.009 $\pm$ 0.002	0	0.033	1.3E-04	4.0E-02	4.0E-02
Gluino charged suppressed ($f = 0.1$) particles with the tracker-only analysis										
400	65	0.300	/	100	17.800 $\pm$ 3.830	13	0.092	9.5E+01	5.5E-02	3.8E-02
600	65	0.300	/	240	1.300 $\pm$ 0.293	0	0.142	9.1E+00	1.3E-02	9.2E-03
1200	65	0.300	/	580	0.030 $\pm$ 0.007	0	0.182	8.4E-02	7.2E-03	7.2E-03
1600	65	0.300	/	670	0.014 $\pm$ 0.003	0	0.137	8.0E-03	9.9E-03	9.9E-03
2000	65	0.300	/	620	0.021 $\pm$ 0.005	0	0.077	9.7E-04	1.7E-02	1.7E-02
2400	65	0.300	/	650	0.016 $\pm$ 0.004	0	0.034	1.3E-04	3.8E-02	3.8E-02
Gluino ($f = 0.5$) particles with the tracker-only analysis										
400	65	0.300	/	30	28.600 $\pm$ 6.100	24	0.094	9.5E+01	6.9E-02	5.5E-02
800	65	0.300	/	330	0.359 $\pm$ 0.079	0	0.128	1.5E+00	1.0E-02	1.0E-02
1200	65	0.300	/	570	0.032 $\pm$ 0.007	0	0.125	8.4E-02	1.1E-02	1.1E-02
1600	65	0.300	/	700	0.011 $\pm$ 0.002	0	0.090	8.0E-03	1.5E-02	1.5E-02
2000	65	0.300	/	730	0.009 $\pm$ 0.002	0	0.045	9.7E-04	2.9E-02	2.9E-02
2400	65	0.300	/	700	0.011 $\pm$ 0.002	0	0.020	1.3E-04	6.6E-02	6.6E-02

obtained from the intersection of the observed limit and the central value of the theoretical cross section.

From the final results, 95% CL limits on the production cross section are shown in Tables 3, 4, 5, and 6 for gluino, stop, stau, and modified Drell–Yan signals, respectively. The limits are determined from the numbers of events passing all final criteria (including the mass criteria). Figure 4 shows the limits as a function of mass for the tracker-only and tracker+TOF analyses. The tracker-only analysis excludes $f = 0.1$ gluino masses below 1590 and 1570 GeV for the cloud interaction model and charge suppression model, respectively. Stop masses below 1020 (970) GeV are excluded for the cloud (charge suppression) models. In addition, the tracker+TOF analysis excludes $\tilde{\tau}_1$ masses below 480(230) GeV for the GMSB (pair production) model. Drell–Yan signals with $|Q| = 1e$ and $2e$ are excluded below 540 and 650 GeV, respectively.

The mass limits obtained at $\sqrt{s} = 13$ TeV for various HSCP signal models are summarized in Table 7, and compared with earlier results at $\sqrt{s} = 7$ and 8 TeV [28]. A significant increase in mass limit is obtained for all models with a significant QCD production cross section (i.e., stops, gluinos, and inclusive production of staus), thanks to the higher center-of-mass energy pp collisions delivered by the LHC. For the $|Q| = 2e$ analysis, results from the previous analysis optimized for multiply charged signals [28] are also provided.

Table 4: Summary of the p_T, I_{as}, $1/\beta$, and mass thresholds, the observed and predicted yields passing these criteria, and the resulting expected (Exp.) and observed (Obs.) cross section limits for stop signals. The signal efficiency and theoretical (Th.) cross section are also listed.

Mass	Requirements				Yields		Signal	σ (pb)		
	p_T (GeV)	I_{as}	$1/\beta$	M (GeV)	Predicted	Data	Eff.	Th.	Exp.	Obs.
Stop particles with the tracker-only analysis										
200	65	0.300	/	0	28.800 $\pm$ 6.140	24	0.194	6.1E+01	3.4E-02	2.5E-02
600	65	0.300	/	20	28.800 $\pm$ 6.140	24	0.260	1.7E-01	2.4E-02	2.0E-02
1000	65	0.300	/	300	0.534 $\pm$ 0.119	0	0.246	6.0E-03	5.2E-03	5.2E-03
1800	65	0.300	/	640	0.018 $\pm$ 0.004	0	0.134	4.6E-05	9.9E-03	9.9E-03
2200	65	0.300	/	660	0.015 $\pm$ 0.003	0	0.064	6.0E-06	2.0E-02	2.0E-02
Stop charged suppressed particles with the tracker-only analysis										
200	65	0.300	/	0	28.800 $\pm$ 6.140	24	0.046	6.1E+01	1.4E-01	1.0E-01
600	65	0.300	/	70	24.000 $\pm$ 5.120	21	0.168	1.7E-01	3.4E-02	2.9E-02
1000	65	0.300	/	300	0.534 $\pm$ 0.119	0	0.188	6.0E-03	7.0E-03	7.0E-03
1800	65	0.300	/	520	0.050 $\pm$ 0.011	0	0.105	4.6E-05	1.2E-02	1.2E-02
2200	65	0.300	/	530	0.046 $\pm$ 0.010	0	0.056	6.0E-06	2.3E-02	2.3E-02

Table 5: Summary of the p_T, I_{as}, $1/\beta$, and mass thresholds, the observed and predicted yields passing these criteria, and the resulting expected (Exp.) and observed (Obs.) cross section limits for stau signals. The signal efficiency and theoretical (Th.) cross section are also listed.

Mass	Requirements				Yields		Signal	σ (pb)		
	p_T (GeV)	I_{as}	$1/\beta$	M (GeV)	Predicted	Data	Eff.	Th.	Exp.	Obs.
Inclusive prod. of stau particles with the tracker+TOF analysis										
200	65	0.175	1.250	50	0.709 $\pm$ 0.143	0	0.290	2.8E-01	6.1E-03	4.4E-03
308	65	0.175	1.250	130	0.055 $\pm$ 0.011	0	0.432	2.5E-02	3.0E-03	3.0E-03
494	65	0.175	1.250	250	0.006 $\pm$ 0.001	0	0.593	1.9E-03	2.2E-03	2.2E-03
651	65	0.175	1.250	350	0.001 $\pm$ 0.000	0	0.663	4.1E-04	1.9E-03	1.9E-03
1029	65	0.175	1.250	590	0.000 $\pm$ 0.000	0	0.712	2.2E-05	1.9E-03	1.9E-03
1599	65	0.175	1.250	890	0.000 $\pm$ 0.000	0	0.521	1.0E-06	2.5E-03	2.5E-03
Pair prod. of stau particles with the tracker+TOF analysis										
200	65	0.175	1.250	50	0.709 $\pm$ 0.143	0	0.242	8.0E-03	7.3E-03	5.3E-03
308	65	0.175	1.250	110	0.091 $\pm$ 0.019	0	0.315	1.5E-03	4.1E-03	4.1E-03
494	65	0.175	1.250	210	0.012 $\pm$ 0.002	0	0.416	1.9E-04	3.2E-03	3.2E-03
651	65	0.175	1.250	310	0.002 $\pm$ 0.000	0	0.497	4.9E-05	2.6E-03	2.6E-03
1029	65	0.175	1.250	550	0.000 $\pm$ 0.000	0	0.591	4.0E-06	2.2E-03	2.2E-03
1599	65	0.175	1.250	890	0.000 $\pm$ 0.000	0	0.474	0.0E+00	2.8E-03	2.8E-03

Table 6: Summary of the p_T, I_{as}, $1/\beta$, and mass thresholds, the observed and predicted yields passing these criteria, and the resulting expected (Exp.) and observed (Obs.) cross section limits for modified Drell–Yan models of various charge signals. The signal efficiency and theoretical (Th.) cross section are also listed.

Mass	Requirements				Yields		Signal	σ (pb)		
	p_T (GeV)	I_{as}	$1/\beta$	M (GeV)	Predicted	Data	Eff.	Th.	Exp.	Obs.
Modified Drell–Yan $\|Q\| = 1e$ particles with the tracker+TOF analysis										
200	65	0.175	1.250	80	0.226 ± 0.046	0	0.304	1.1E-01	4.4E-03	4.4E-03
400	65	0.175	1.250	200	0.014 ± 0.003	0	0.417	7.3E-03	3.2E-03	3.2E-03
600	65	0.175	1.250	320	0.002 ± 0.000	0	0.462	1.2E-03	2.9E-03	2.9E-03
800	65	0.175	1.250	460	0.000 ± 0.000	0	0.486	2.6E-04	2.8E-03	2.8E-03
1000	65	0.175	1.250	590	0.000 ± 0.000	0	0.486	7.6E-05	2.9E-03	2.9E-03
1800	65	0.175	1.250	1010	0.000 ± 0.000	0	0.250	1.0E-06	5.5E-03	5.5E-03
2600	65	0.175	1.250	1230	0.000 ± 0.000	0	0.026	0.0E+00	5.6E-02	5.6E-02
Modified Drell–Yan $\|Q\| = 2e$ particles with the tracker+TOF analysis										
200	65	0.175	1.250	0	0.901 ± 0.182	0	0.211	3.0E-01	8.7E-03	6.1E-03
400	65	0.175	1.250	90	0.164 ± 0.033	0	0.410	2.3E-02	3.2E-03	3.2E-03
600	65	0.175	1.250	200	0.014 ± 0.003	0	0.482	3.5E-03	2.8E-03	2.8E-03
800	65	0.175	1.250	300	0.003 ± 0.001	0	0.488	8.0E-04	2.6E-03	2.6E-03
1000	65	0.175	1.250	370	0.001 ± 0.000	0	0.450	2.4E-04	3.0E-03	3.0E-03
1800	65	0.175	1.250	420	0.001 ± 0.000	0	0.141	4.0E-06	9.6E-03	9.6E-03
2600	65	0.175	1.250	540	0.000 ± 0.000	0	0.040	0.0E+00	3.3E-02	3.3E-02

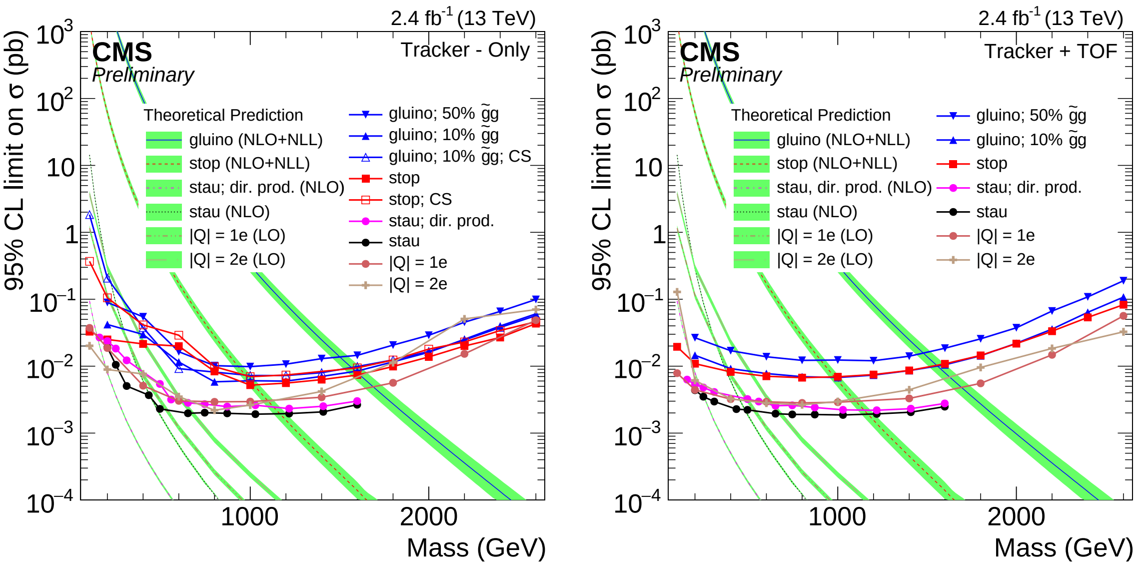

Figure 4: Cross section upper limits at 95% CL on various signal models for the tracker-only analysis (left) and tracker+TOF analysis (right) at $\sqrt{s} = 13$ TeV. In the legend, 'CS' stands for charged suppressed interaction model.

Table 7: Mass limits obtained at $\sqrt{s} = 13\,\text{TeV}$ for various HSCP candidate models compared with earlier results for $\sqrt{s} = 7+8\,\text{TeV}$ [28]. In the model name, 'CS' stands for charged suppressed interaction model. The limits for doubly charged particles are also compared to the earlier results obtained with the 'multiply charged' analysis that was specifically designed to search for multiply charged particles.

Model	analysis used	$\sqrt{s} = 7+8$ TeV	$\sqrt{s} = 13$ TeV
Gluino $f = 0.1$	tracker-only	$M > 1320$ GeV	$M > 1590$ GeV
	tracker+TOF	$M > 1290$ GeV	$M > 1560$ GeV
Gluino $f = 0.1$ CS	tracker-only	$M > 1230$ GeV	$M > 1570$ GeV
Gluino $f = 0.5$	tracker-only	$M > 1260$ GeV	$M > 1500$ GeV
	tracker+TOF	$M > 1220$ GeV	$M > 1480$ GeV
Gluino $f = 0.5$ CS	tracker-only	$M > 1150$ GeV	$M > 1530$ GeV
Stop	tracker-only	$M > 940$ GeV	$M > 1020$ GeV
	tracker+TOF	$M > 910$ GeV	$M > 980$ GeV
Stop CS	tracker-only	$M > 820$ GeV	$M > 970$ GeV
Stau inc. prod. (GMSB SPS7)	tracker+TOF	$M > 440$ GeV	$M > 480$ GeV
	tracker-only	$M > 390$ GeV	$M > 450$ GeV
Stau pair prod.	tracker+TOF	$M > 340$ GeV	$M > 230$ GeV
	tracker-only	$M > 190$ GeV	
DY $Q = 1e$	tracker-only	$M > 650$ GeV	$M > 510$ GeV
	tracker+TOF	$M > 650$ GeV	$M > 540$ GeV
DY $Q = 2e$	multiply charged	$M > 730$ GeV	-
	tracker-only	$M > 520$ GeV	$M > 600$ GeV
	tracker+TOF	$M > 520$ GeV	$M > 650$ GeV

8 Summary

A number of searches for heavy stable charged particles produced in pp collisions at $\sqrt{s} = 13\,\text{TeV}$ using the CMS detector have been presented. Two complementary analyses are performed: a search using only the tracker and a search using both the tracker and the muon system. Data are found to be compatible with the background expectation. Mass limits for gluinos, stops, staus, and multiply charged particles are calculated. The models for R-hadron-like HSCPs include a varying fraction of $\tilde{g}-$gluon production and two different interaction models producing a variety of exotic experimental signatures. The limits, ranging up to 1590 GeV for gluinos, are the most restrictive to date, clearly improving previous limits from the LHC.

References

[1] M. Drees and X. Tata, "Signals for heavy exotics at hadron colliders and supercolliders", *Phys. Lett. B* **252** (1990) 695, doi:10.1016/0370-2693(90)90508-4.

[2] M. Fairbairn et al., "Stable massive particles at colliders", *Phys. Rept.* **438** (2007) 1, doi:10.1016/j.physrep.2006.10.002, arXiv:hep-ph/0611040.

[3] C. W. Bauer et al., "Supermodels for early LHC", *Phys. Lett. B* **690** (2010) 280, doi:10.1016/j.physletb.2010.05.032, arXiv:0909.5213.

[4] A. Kusenko and M. E. Shaposhnikov, "Supersymmetric Q-balls as dark matter", *Phys. Lett. B* **418** (1998) 46, doi:10.1016/S0370-2693(97)01375-0, arXiv:hep-ph/9709492.

[5] B. Koch, M. Bleicher, and H. Stoecker, "Black holes at LHC?", *J. Phys. G* **34** (2007) S535, doi:10.1088/0954-3899/34/8/S44, arXiv:hep-ph/0702187.

[6] J. S. Schwinger, "Magnetic charge and quantum field theory", *Phys. Rev.* **144** (1966) 1087, doi:10.1103/PhysRev.144.1087.

[7] D. Fargion, M. Khlopov, and C. A. Stephan, "Cold dark matter by heavy double charged leptons?", *Class. Quant. Grav.* **23** (2006) 7305, doi:10.1088/0264-9381/23/24/008, arXiv:astro-ph/0511789.

[8] Particle Data Group Collaboration, "Review of Particle Physics (RPP)", *Phys. Rev. D* **86** (2012) 010001, doi:10.1103/PhysRevD.86.010001.

[9] ALEPH Collaboration, "Search for pair production of longlived heavy charged particles in e^+e^- annihilation", *Phys. Lett. B* **405** (1997) 379, doi:10.1016/S0370-2693(97)00715-6, arXiv:hep-ex/9706013.

[10] DELPHI Collaboration, "Search for heavy stable and longlived particles in e^+e^- collisions at $\sqrt{s} = 189\,\text{GeV}$", *Phys. Lett. B* **478** (2000) 65, doi:10.1016/S0370-2693(00)00265-3, arXiv:hep-ex/0103038.

[11] L3 Collaboration, "Search for heavy neutral and charged leptons in e^+e^- annihilation at LEP", *Phys. Lett. B* **517** (2001) 75, doi:10.1016/S0370-2693(01)01005-X, arXiv:hep-ex/0107015.

[12] OPAL Collaboration, "Search for stable and longlived massive charged particles in e^+e^- collisions at $\sqrt{s} = 130$ GeV to 209 GeV", *Phys. Lett. B* **572** (2003) 8, doi:10.1016/S0370-2693(03)00639-7, arXiv:hep-ex/0305031.

[13] H1 Collaboration, "Measurement of anti-deuteron photoproduction and a search for heavy stable charged particles at HERA", *Eur. Phys. J. C* **36** (2004) 413, doi:10.1140/epjc/s2004-01894-1, arXiv:hep-ex/0403056.

[14] CDF Collaboration, "Search for long-lived massive charged particles in 1.96 TeV $\bar{p}p$ collisions", *Phys. Rev. Lett.* **103** (2009) 021802, doi:10.1103/PhysRevLett.103.021802, arXiv:0902.1266.

[15] D0 Collaboration, "Search for long-lived charged massive particles with the D0 detector", *Phys. Rev. Lett.* **102** (2009) 161802, doi:10.1103/PhysRevLett.102.161802, arXiv:0809.4472.

[16] D0 Collaboration, "A search for charged massive long-lived particles", *Phys. Rev. Lett.* **108** (2012) 121802, doi:10.1103/PhysRevLett.108.121802, arXiv:1110.3302.

[17] D0 Collaboration, "Search for charged massive long-lived particles at $\sqrt{s} = 1.96$ TeV", *Phys. Rev. D* **87** (2013), no. 5, 052011, doi:10.1103/PhysRevD.87.052011, arXiv:1211.2466.

[18] ATLAS Collaboration, "Search for heavy long-lived charged particles with the ATLAS detector in pp collisions at $\sqrt{s} = 7$ TeV", *Phys. Lett. B* **703** (2011) 428, doi:10.1016/j.physletb.2011.08.042, arXiv:1106.4495.

[19] ATLAS Collaboration, "Search for stable hadronising squarks and gluinos with the ATLAS experiment at the LHC", *Phys. Lett. B* **701** (2011) 1, doi:10.1016/j.physletb.2011.05.010, arXiv:1103.1984.

[20] ATLAS Collaboration, "Search for massive long-lived highly ionising particles with the ATLAS detector at the LHC", *Phys. Lett. B* **698** (2011) 353, doi:10.1016/j.physletb.2011.03.033, arXiv:1102.0459.

[21] ATLAS Collaboration, "Searches for heavy long-lived sleptons and R-Hadrons with the ATLAS detector in pp collisions at $\sqrt{s} = 7$ TeV", *Phys. Lett. B* **720** (2013) 277, doi:10.1016/j.physletb.2013.02.015, arXiv:1211.1597.

[22] ATLAS Collaboration, "Search for long-lived, multi-charged particles in pp collisions at $\sqrt{s}$=7 TeV using the ATLAS detector", *Phys. Lett.* **B722** (2013) 305, doi:10.1016/j.physletb.2013.04.036, arXiv:1301.5272.

[23] CMS Collaboration, "Search for heavy stable charged particles in pp collisions at $\sqrt{s} = 7$ TeV", *JHEP* **03** (2011) 024, doi:10.1007/JHEP03(2011)024, arXiv:1101.1645.

[24] CMS Collaboration, "Search for fractionally charged particles in pp collisions at $\sqrt{s} = 7$ TeV", *Phys. Rev. Lett.* (2012) arXiv:1210.2311.

[25] CMS Collaboration, "Search for heavy long-lived charged particles in pp collisions at $\sqrt{s} = 7$ TeV", *Phys. Lett. B* **713** (2012) 408, doi:10.1016/j.physletb.2012.06.023, arXiv:1205.0272.

[26] C. F. Berger, J. S. Gainer, J. L. Hewett, and T. G. Rizzo, "Supersymmetry without prejudice", *JHEP* **02** (2009) 023, doi:10.1088/1126-6708/2009/02/023, arXiv:0812.0980.

[27] M. W. Cahill-Rowley, J. L. Hewett, A. Ismail, and T. G. Rizzo, “More energy, more searches, but the phenomenological MSSM lives on”, *Phys. Rev. D* **88** (2013), no. 3, 035002, doi:10.1103/PhysRevD.88.035002, arXiv:1211.1981.

[28] CMS Collaboration, “Searches for long-lived charged particles in pp collisions at $\sqrt{s} = 7$ and 8 TeV”, *JHEP* **07** (2013) 122, doi:10.1007/JHEP07(2013)122, arXiv:1305.0491.

[29] T. Sjöstrand, S. Mrenna, and P. Z. Skands, “A brief introduction to PYTHIA 8.1”, *Comput. Phys. Commun.* **178** (2008) 852, doi:10.1016/j.cpc.2008.01.036, arXiv:0710.3820.

[30] A. C. Kraan, “Interactions of heavy stable hadronizing particles”, *Eur. Phys. J. C* **37** (2004) 91, doi:10.1140/epjc/s2004-01997-7, arXiv:hep-ex/0404001.

[31] R. Mackeprang and A. Rizzi, “Interactions of coloured heavy stable particles in matter”, *Eur. Phys. J. C* **50** (2007) 353, doi:10.1140/epjc/s10052-007-0252-4, arXiv:hep-ph/0612161.

[32] G. Giudice and R. Rattazzi, “Theories with gauge mediated supersymmetry breaking”, *Phys. Rept.* **322** (1999) 419, doi:10.1016/S0370-1573(99)00042-3, arXiv:hep-ph/9801271.

[33] B. Allanach et al., “The Snowmass points and slopes: Benchmarks for SUSY searches”, *Eur. Phys. J. C* **25** (2002) 113, doi:10.1007/s10052-002-0949-3, arXiv:hep-ph/0202233.

[34] F. E. Paige, S. D. Protopopescu, H. Baer, and X. Tata, “ISAJET 7.69: A Monte Carlo Event Generator for pp, $\bar{p}p$, and e^+e^- Reactions”, (2003). arXiv:hep-ph/0312045.

[35] CMS Collaboration, “The CMS experiment at the CERN LHC”, *JINST* **3** (2008) S08004, doi:10.1088/1748-0221/3/08/S08004.

[36] CMS Collaboration, “Description and performance of track and primary-vertex reconstruction with the CMS tracker”, *JINST* **9** (2014) P10009, doi:10.1088/1748-0221/9/10/P10009, arXiv:1405.6569.

[37] CMS Collaboration, “Performance of CMS muon reconstruction in pp collision events at $\sqrt{s} = 7$ TeV”, *JINST* **7** (2012) P10002, doi:10.1088/1748-0221/7/10/P10002, arXiv:1206.4071.

[38] CMS Collaboration, “Jet performance in pp collisions at $\sqrt{s}$=7 TeV”, CMS Physics Analysis Summary CMS-PAS-JME-10-003, CMS, 2010.

[39] CMS Collaboration, “Particle–flow event reconstruction in CMS and performance for jets, taus, and $E_{\mathrm{T}}^{\mathrm{miss}}$”, CMS Physics Analysis Summary CMS-PAS-PFT-09-001, CERN, 2009.

[40] CMS Collaboration, “Measurement of tracking efficiency”, CMS Physics Analysis Summary CMS-PAS-TRK-10-002, CMS, 2010.

[41] T. Junk, “Confidence level computation for combining searches with small statistics”, *Nucl. Instrum. Meth. A* **434** (1999) 435, doi:10.1016/S0168-9002(99)00498-2, arXiv:hep-ex/9902006.

[42] A. L. Read, "Presentation of search results: the CL_s technique", *J. Phys. G* **28** (2002) 2693, doi:10.1088/0954-3899/28/10/313.

[43] G. Cowan, K. Cranmer, E. Gross, and O. Vitells, "Asymptotic formulae for likelihood-based tests of new physics", *Eur. Phys. J. C* **71** (2011) 1554, doi:10.1140/epjc/s10052-011-1554-0, arXiv:1007.1727.

[44] W. T. Eadie et al., "Statistical methods in experimental physics". North Holland, Amsterdam, 1971.

[45] F. James, "Statistical methods in experimental physics". World Scientific, Singapore, 2006.

[46] A. Kulesza and L. Motyka, "Threshold resummation for squark-antisquark and gluino-pair production at the LHC", *Phys. Rev. Lett.* **102** (2009) 111802, doi:10.1103/PhysRevLett.102.111802, arXiv:0807.2405.

[47] A. Kulesza and L. Motyka, "Soft gluon resummation for the production of gluino-gluino and squark-antisquark pairs at the LHC", *Phys. Rev. D* **80** (2009) 095004, doi:10.1103/PhysRevD.80.095004, arXiv:0905.4749.

[48] W. Beenakker et al., "Soft-gluon resummation for squark and gluino hadroproduction", *JHEP* **12** (2009) 041, doi:10.1088/1126-6708/2009/12/041, arXiv:0909.4418.

[49] W. Beenakker et al., "Supersymmetric top and bottom squark production at hadron colliders", *JHEP* **08** (2010) 098, doi:10.1007/JHEP08(2010)098, arXiv:1006.4771.

[50] W. Beenakker, R. Hopker, and M. Spira, "PROSPINO: A program for the PROduction of Supersymmetric Particles In Next-to-leading Order QCD", arXiv:hep-ph/9611232.

[51] P. M. Nadolsky et al., "Implications of CTEQ global analysis for collider observables", *Phys. Rev. D* **78** (2008) 013004, doi:10.1103/PhysRevD.78.013004, arXiv:0802.0007.